

ANALYTICAL SOLUTION FOR FREE VIBRATION ANALYSIS OF GPL-RP BEAM INTEGRATED WITH PIEZOELECTRIC LAYERS

Tran Quang Hung¹ , Tran Minh Tu² , Do Minh Duc^{1,*}

¹*The University of Da Nang, University of Science and Technology, Da Nang, Vietnam*

²*Hanoi University of Civil Engineering, Hanoi, Vietnam*

*E-mail: ducdhbk@gmail.com

Received: 01 December 2022 / Published online: 30 December 2022

Abstract. This report presents an analytical approach to the natural frequency analysis of a porous beam consisting of a host porous layer reinforced with graphene platelets (GPLs), namely GPL-reinforced porous core, and two piezoelectric outer layers. In the modelling, symmetric distributions of both porosity and GPLs in the core are supposed. The effective mechanical properties of the GPL-reinforced porous core are estimated by Halpin–Tsai model and the rule of mixture. The electric potential in each piezoelectric layer is assumed to vary linearly across its thickness. Two types of electrical boundary conditions, which are open- and closed-circuits, are considered for the free surfaces of the piezoelectric layers. Parabolic shear deformation beam theory associated with Hamilton’s principle is adopted to derive the governing equations of the free vibration. Afterwards these equations are solved analytically by Navier’s solution. Comparative and comprehensive studies are carried out to examine the accuracy and effects of parameters and conditions, such as GPL weight fraction, porosity coefficient, and electrical boundary conditions on the natural frequencies of the beam.

Keywords: piezoelectric material, porous beam, graphene platelets, Navier’s solution.

1. INTRODUCTION

Structures that are made of porous material reinforced with GPLs, shorten as GPL-RP structures, are a novel form of modern lightweight structures. The advantage of these structures is due to the combination of the good features of porous material, such as lightweight, thermal and acoustic insulation and energy dissipation, with the high strength and high modulus of GPLs. Studies have shown that by reinforcing porous materials with a small amount of GPLs, the stiffness of porous structures is considerably enhanced while the lightweight ability of structures is still maintained. Thus, GPL-RP structures, have attracted great attention from researchers. For example, the post-buckling of a GPL-RP beam, considering geometrical imperfection and elastic foundation, was reported in Ref. [1] for the classical beam model and in Ref. [2] for the refined shear deformable

model by Barati and Zenkour. Ganapathi et al. [3] studied the dynamic response of GPL-RP curved beam by Navier's solution. Gao et al. [4] investigated the effects of stochastic porosity distributions, GPL dispersion patterns, as well as random material properties on the stability capacities of GPL-RP beams. Using the nonlocal strain gradient theory, Sahmani et al. [5] performed the nonlinear bending of GPL-RP micro/nano-beams. Anirudh et al. [6] analyzed the bending, free vibration and buckling behavior of GPL-RP curved beams by finite element method based on a 3-node curved beam element. Kitipornchai et al. [7] studied the fundamental frequency and the critical buckling load of GPL-RP beams with different combinations of GPL and porosity distributions. Using quasi-3D beam theory, which includes both shear strain and thickness stretching effect, Priyanka et al. [8] investigated the free vibration and buckling of GPL-RP beam under axially variable loads. Xu et al. [9] analyzed the free vibration of GPL-RP beam with spinning movement by the differential transformation method. All the above-mentioned works focus on GPL-RP beams. Numerous studies on GPL-RP plates and shells were gathered and presented in the review papers by Kiarasi et al. [10] and by Zhao et al. [11].

Recently, integrating piezoelectric layers into host porous/GPL-RP structures to actively control and reduce unexpected mechanical responses has also received high attention from the scientific community. Several studies have been conducted to investigate mechanical behavior of such structures available in the literature. Nguyen et al. [12] studied the dynamic responses and active vibration control of GPL-RP plates integrated with piezoelectric sensor and actuator layers. Bending and transient responses of GPL-RP plates embedded in piezoelectric layers were conducted by Nguyen et al. [13] using isogeometric analysis (IGA). Nguyen et al. [14] presented the geometrically nonlinear static and dynamic analyses of GPL-RP plates integrated with smart piezoelectric layers. Hao et al. [15] studied the active vibration control of a porous truncated conical shell integrated with smart sensor and actuator layers under impact loadings.

The above literature survey reveals that researches on GPL-RP structures integrated with piezoelectric layers are still at the infancy stage and very limited. No report on such beam-like structures is available in the open literature. To fill the existing research gap, this study deals with free vibration of GPL-RP beam covered by two piezoelectric face layers, shortened as piezoelectric GPL-RP beam, by analytical approach. The distributions of porosity and GPLs in the beam are assumed to be symmetrical in the analysis. The effective mechanical properties of the GPL-reinforced porous core are estimated via Halpin-Tsai model and the rule of mixture. The distribution of electric potential across the thickness of each piezoelectric layer is assumed to be linear. In addition, open- and closed-circuit conditions are considered for the free surfaces of the piezoelectric layers. Parabolic shear deformation beam theory associated with Hamilton's principle is adopted to derive the governing equations of the free vibration. These equations are then solved analytically by Navier's method. A comparative study is conducted to validate the developed formulations. Parametric study is carried out to examine the effects of key parameters and conditions, such as GPL weight fraction, porosity coefficient and electrical boundary conditions on the natural frequencies of the beam.

2. THEORY AND FORMULATIONS

2.1. Configuration and geometrical parameters

Consider a piezoelectric GPL-RP beam, as illustrated in Fig. 1(a). The beam has the dimensions of $L \times h \times b$ and consists of three layers. The host porous core, thickness h_c , is made of metal foam reinforced with GPLs and two piezoelectric face layers, thickness h_f . The total thickness of the beam is $h = h_c + 2 \times h_f$.

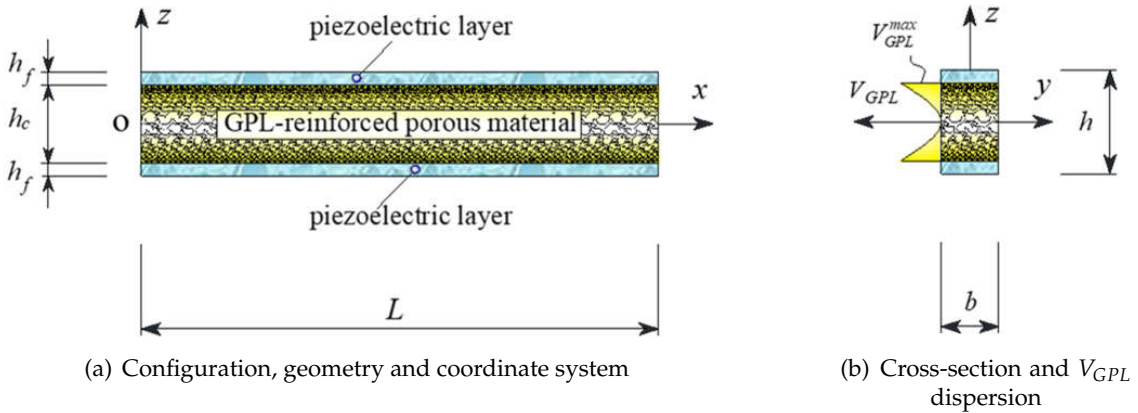


Fig. 1. Configuration, porosity distribution and GPL dispersion of piezoelectric GPL-RP beam

2.2. Effective material properties

2.2.1. Piezoelectric outer layers

The material of the piezoelectric face layers is assumed to be homogeneous. Hence, elastic moduli E and G , mass density ρ , Poisson's ratio μ , piezoelectric stress constant e and dielectric permittivity constant p are unchanged.

2.2.2. GPL-reinforced porous core

The porous core is made of porous material strengthened by reinforcing GPLs. There are many types of porosity and GPL distributions which can be designed for porous material reinforced with GPLs. They have significant effect on the stiffness of GPL-RP structures. Various studies, e.g., [1–3, 7, 8], show that both symmetric distributions of pores and GPLs in which the presence of low porosity and high content of GPLs far from the neutral surface is the most effective way to enhance the stiffness of the system. Thus, both symmetric distributions of porosity and GPLs are supposed in this study. The distribution of pores as well as GPLs are illustrated in Fig. 1. Consequently, the effective material properties, such as elastic moduli $E(z)$ and $G(z)$, and mass density $\rho(z)$, can be defined as functions of variable z below [7]

$$\begin{cases} E(z) = \hat{E} [1 - e_o \xi(z)] \\ G(z) = E(z) / [2 + 2\mu(z)] \\ \rho(z) = \hat{\rho} [1 - e_m \xi(z)] \\ \xi(z) = \cos(\pi z / h_c) \end{cases} \quad -h_c/2 \leq z \leq h_c/2 \quad (1)$$

where \hat{E} and $\hat{\rho}$ denote Young's modulus and mass density of GPL-reinforced metal foam without internal pores, respectively; e_o is the porosity coefficient; e_m is the coefficient of mass density which could be determined via the porosity coefficient e_o by the relation below [7]

$$= \frac{1.121}{\xi(z)} \left[1 - \sqrt[2.3]{1 - e_o \xi(z)} \right]. \quad (2)$$

Meanwhile, the volume fraction of GPLs, denoted as V_{GPL} and illustrated in Fig. 1(b), can be defined as [7]

$$V_{GPL}(z) = V_{GPL}^{\max} [1 - \cos(\pi z / h_c)], \quad -h_c/2 \leq z \leq h_c/2, \quad (3)$$

where V_{GPL}^{\max} are the peak volume fraction value of GPLs. It is determined by the relation between the volume fraction V_{GPL} and weight fraction W_{GPL} of GPLs by following equation [7]

$$\frac{\rho_m W_{GPL}}{\rho_m W_{GPL} + \rho_{GPL} - \rho_{GPL} W_{GPL}} \int_{-h_c/2}^{h_c/2} [1 - e_m \xi(z)] dz = \int_{-h_c/2}^{h_c/2} [1 - e_m \xi(z)] V_{GPL}(z) dz, \quad (4)$$

in which ρ_m and ρ_{GPL} are mass density of metal matrix and GPLs, respectively.

The elastic modulus \hat{E} of GPL-reinforced material without pores can be estimated based on Halpin-Tsai micromechanics model [16]

$$\hat{E} = \left[\frac{3}{8} \times \left(\frac{1/\eta_L + \zeta_L V_{GPL}}{1/\eta_L - V_{GPL}} \right) + \frac{5}{8} \times \left(\frac{1/\eta_W + \zeta_W V_{GPL}}{1/\eta_W - V_{GPL}} \right) \right] E_m. \quad (5)$$

The coefficients in Eq. (5) are determined via the mechanical properties and geometrical parameters of the metal matrix and GPLs by the relations:

$$\zeta_L = 2 \times \frac{l_{GPL}}{t_{GPL}}, \quad \zeta_W = 2 \times \frac{w_{GPL}}{t_{GPL}}, \quad \eta_L = \frac{E_{GPL} - E_m}{E_{GPL} + \zeta_L E_m}, \quad \eta_W = \frac{E_{GPL} - E_m}{E_{GPL} + \zeta_W E_m}. \quad (6)$$

In addition, the mass density $\hat{\rho}$ and Poisson's ratio $\hat{\mu}$ of GPL-reinforced material without pores can be determined by the rule of mixtures [11]

$$\begin{cases} \hat{\rho} = \rho_{GPL} V_{GPL} + \rho_m (1 - V_{GPL}) \\ \hat{\mu} = \mu_{GPL} V_{GPL} + \mu_m (1 - V_{GPL}) \end{cases} \quad (7)$$

In Eqs. (5)–(7), E_m, ρ_m and μ_m are, respectively, the elastic modulus, mass density and Poisson's ratio of the metal matrix; similarly, E_{GPL}, ρ_{GPL} and μ_{GPL} are those of GPLs; $l_{GPL}, t_{GPL}, w_{GPL}$ represent the average length, thickness and width of GPLs, respectively.

Poisson's ratio of GPL-reinforced porous core is also estimated as [7]

$$\mu(z) = 0.221 e_m \xi(z) + \hat{\mu} \left[0.342 \{ e_m \xi(z) \}^2 - 1.21 e_m \xi(z) + 1 \right]. \quad (8)$$

2.3. Displacement field, strain field and constitutive equation

In this work, the parabolic shear deformation beam theory (PSBT) is adopted to model the beam. The displacement components u and w , which are, respectively, in the x - and z -directions, can be expressed as

$$\begin{cases} u(x, z, t) = u_o(x, t) - z \frac{\partial w_o(x, t)}{\partial x} + \Phi(z) \varphi_{os}(x, t) \\ w(x, z, t) = w_o(x, t) \\ \Phi(z) = z - 4z^3 / (3h^2) \end{cases} \quad (9)$$

in which u_o , w_o and φ_{os} are, respectively, the displacements in the x -, z -directions and the transverse shear strain of an arbitrary point on the mid-surface ($z = 0$); t stands for the time.

The strain field can be derived from the displacement components by

$$\varepsilon_x = \frac{\partial u}{\partial x} = \frac{\partial u_o}{\partial x} - z \frac{\partial^2 w_o}{\partial x^2} + \Phi \frac{\partial \varphi_{os}}{\partial x}, \quad \gamma_{xz} = \frac{\partial u}{\partial z} + \frac{\partial w}{\partial x} = \frac{\partial \Phi}{\partial z} \varphi_{os}, \quad (10)$$

where ε_x and γ_{xz} are the axial and shear strains, respectively.

The linear piezoelectric constitutive equation expressing the electrical and mechanical interactions for one-dimensional (1D) beam problem has the form as [17]

$$\begin{Bmatrix} \sigma_x \\ \tau_{xz} \\ D_z \end{Bmatrix} \begin{bmatrix} E & 0 & -e_{31} \\ 0 & G & 0 \\ e_{31} & 0 & p_{33} \end{bmatrix} \begin{Bmatrix} \varepsilon_x \\ \gamma_{xz} \\ E_z \end{Bmatrix}, \quad (11)$$

where σ_x , τ_{xz} are the axial and shear stresses, respectively; E and G are Young's modulus and shear modulus, respectively; e_{31} is the piezoelectric stress constant; D_z is the electric displacement; p_{33} is the dielectric permittivity constant; E_z is the electric field.

Assuming that the electric potential field varies according to a linear function along the thickness of each piezoelectric layer [18, 19]. The electric field E_z can be determined as [20]

$$E_z = -\phi_o(x, t) / h_f, \quad (12)$$

where $\phi_o(x, t)$ is the electric potential difference between the top and bottom surfaces of the considered piezoelectric layer, and h_f is its layer thickness.

Evidently, the constitutive relations of Eq. (11) can also be used for the non-piezoelectric material of the porous core by ignoring all the electric terms.

2.4. Energy expressions

The variation of the strain energy can be stated as

$$\begin{aligned} \delta U &= \int_0^L \int_A (\sigma_x \delta \varepsilon_x + \tau_{xz} \delta \gamma_{xz} - D_z \delta E_z) dA dx \\ &= \int_0^L \left(N \frac{\partial \delta u_o}{\partial x} - M_b \frac{\partial^2 \delta w_o}{\partial x^2} + M_s \frac{\partial \delta \varphi_{os}}{\partial x} + Q \delta \varphi_{os} + B_{E1} \delta \phi_o^t + B_{E2} \delta \phi_o^b \right) dx. \end{aligned} \quad (13)$$

The stress and electric displacement resultants are defined as

$$\{N, M_b, M_s, Q, B_{E1}, B_{E2}\} = \int_A \left\{ \sigma_x, z\sigma_x, \Phi\sigma_x, \tau_{xz}, \frac{\partial\Phi}{\partial z}, \frac{D_z^t}{h_f}, \frac{D_z^b}{h_f} \right\} dA. \quad (14)$$

In Eqs. (13) and (14), $\phi_o^t(x, t)$ and $\phi_o^b(x, t)$ are the electric potential differences corresponding to the top and bottom piezoelectric layers, respectively; A is the area of the beam cross-section and L is the length of the beam.

By substituting Eqs. (10) and (11) into Eq. (14), the stress and electric displacement resultants can be expressed by matrix form

$$\begin{Bmatrix} N \\ M_b \\ M_s \\ Q \\ B_{E1} \\ B_{E2} \end{Bmatrix} = \begin{bmatrix} A_1 & B_1 & B_s & 0 \\ B_1 & D & D_s & 0 \\ B_s & D_s & H_s & 0 \\ 0 & 0 & 0 & A_s \\ D_1^t & D_2^t & D_3^t & 0 \\ D_1^b & D_2^b & D_3^b & 0 \end{bmatrix} \begin{Bmatrix} \partial u_o / \partial x \\ -\partial^2 w_o / \partial x^2 \\ \partial \varphi_{os} / \partial x \\ \varphi_{os} \end{Bmatrix} + \begin{bmatrix} D_1^t & D_1^b \\ D_2^t & D_2^b \\ D_3^t & D_3^b \\ 0 & 0 \\ -D_5^t & 0 \\ 0 & -D_6^b \end{bmatrix} \begin{Bmatrix} \phi_o^t \\ \phi_o^b \end{Bmatrix} \quad (15)$$

where

$$\{A_1, B_1, D, B_s, D_s, H_s, A_s\} = \int_A E(z) \left\{ 1, z, z^2, \Phi, z\Phi, \Phi^2, \frac{1}{2+2\mu} \left(\frac{\partial\Phi}{\partial z} \right)^2 \right\} dA, \quad (16)$$

$$\begin{aligned} \{D_1^t, D_2^t, D_3^t, D_5^t\} &= b \int_{h_c/2}^{h/2} \frac{e_{31}}{h_f} \left\{ 1, z, \Phi, \frac{p_{33}}{e_{31}h_f} \right\} dz, \\ \{D_1^b, D_2^b, D_3^b, D_6^b\} &= b \int_{-h/2}^{-h_c/2} \frac{e_{31}}{h_f} \left\{ 1, z, \Phi, \frac{p_{33}}{e_{31}h_f} \right\} dz. \end{aligned} \quad (17)$$

The variation of kinetic energy of the beam can be stated as

$$\begin{aligned} \delta K &= \int_0^L \int_A \rho(z) (\dot{u}\delta\dot{u} + \dot{w}\delta\dot{w}) dA dx \\ &= \int_0^L I_o (\dot{u}_o\delta\dot{u}_o + \dot{w}_o\delta\dot{w}_o) dx - \int_0^L I_1 \left(\dot{u}_o \frac{\partial\delta\dot{w}_o}{\partial x} + \frac{\partial\dot{w}_o}{\partial x} \delta\dot{u}_o \right) dx \\ &\quad + \int_0^L I_2 \left(\frac{\partial\dot{w}_o}{\partial x} \frac{\partial\delta\dot{w}_o}{\partial x} \right) dx + \int_0^L I_1 (\dot{u}_o\delta\dot{\varphi}_{os} + \dot{\varphi}_{os}\delta\dot{u}_o) dx \\ &\quad - \int_0^L I_2 \left(\frac{\partial\dot{w}_o}{\partial x} \delta\dot{\varphi}_{os} + \dot{\varphi}_{os} \frac{\partial\delta\dot{w}_o}{\partial x} \right) dx + \int_0^L I_3 \dot{\varphi}_{os}\delta\dot{\varphi}_{os} dx, \end{aligned} \quad (18)$$

where

$$\{I_0, I_1, I_2, J_1, J_2, J_3\} = \int_A \rho(z) \{1, z, z^2, \Phi, z\Phi, \Phi^2\} dA. \quad (19)$$

2.5. Hamilton's principle and governing equations

Hamilton's principle is used to derive the governing equations of the piezoelectric GPL-RP beam. This principle can be expressed for the case of the free vibration as

$$\int_{t_1}^{t_2} (\delta U - \delta K) dt = 0. \quad (20)$$

Substituting the expressions δU and δK from Eqs. (13) and (18) into Eq. (20), then integrating by parts and collecting the coefficients of δu_o , δw_o , $\delta \varphi_{os}$, ϕ_o^t and ϕ_o^b drive the governing equations of the system. Next, substituting the stress and electric displacement resultants of Eq. (15) into them, the governing equations can be obtained in terms of the displacements and electric potential differences as

$$\begin{cases} A_1 \frac{\partial^2 u_o}{\partial x^2} - B_1 \frac{\partial^3 w_o}{\partial x^3} + B_s \frac{\partial^2 \varphi_{os}}{\partial x^2} + D_1^t \frac{\partial \phi_o^t}{\partial x} + D_1^b \frac{\partial \phi_o^b}{\partial x} = I_0 \ddot{u}_o - I_1 \frac{\partial \ddot{w}_o}{\partial x} + J_1 \ddot{\varphi}_{os}, \\ B_1 \frac{\partial^3 u_o}{\partial x^3} - D \frac{\partial^4 w_o}{\partial x^4} + D_s \frac{\partial^3 \varphi_{os}}{\partial x^3} + D_2^t \frac{\partial^2 \phi_o^t}{\partial x^2} + D_2^b \frac{\partial^2 \phi_o^b}{\partial x^2} = I_0 \ddot{w}_o + I_1 \frac{\partial \ddot{u}_o}{\partial x} - I_2 \frac{\partial^2 \ddot{w}_o}{\partial x^2} + J_2 \frac{\partial \ddot{\varphi}_{os}}{\partial x}, \\ B_s \frac{\partial^2 u_o}{\partial x^2} - D_s \frac{\partial^3 w_o}{\partial x^3} + H_s \frac{\partial^2 \varphi_{os}}{\partial x^2} - A_s \varphi_{os} + D_3^t \frac{\partial \phi_o^t}{\partial x} + D_3^b \frac{\partial \phi_o^b}{\partial x} = J_1 \ddot{u}_o - J_2 \frac{\partial \ddot{w}_o}{\partial x} + J_3 \ddot{\varphi}_{os}, \\ D_1^t \frac{\partial u_o}{\partial x} - D_2^t \frac{\partial^2 w_o}{\partial x^2} + D_3^t \frac{\partial \varphi_{os}}{\partial x} - D_5^t \phi_o^t = 0, \\ D_1^b \frac{\partial u_o}{\partial x} - D_2^b \frac{\partial^2 w_o}{\partial x^2} + D_3^b \frac{\partial \varphi_{os}}{\partial x} - D_6^b \phi_o^b = 0. \end{cases} \quad (21)$$

2.6. Analytical solution

Navier's method based on Fourier series is used to determine the analytical solution for a simply supported beam. Assuming each of the unknown components u_o , w_o , φ_{os} , ϕ_o^t and ϕ_o^b is trigonometric series, which satisfies the edge conditions, as follows

$$\begin{cases} u_o(x, t) = \sum_{n=1}^{\infty} U_n e^{i\omega t} \cos(\alpha x), & w_o(x, t) = \sum_{n=1}^{\infty} W_n e^{i\omega t} \sin(\alpha x), \\ \varphi_{os}(x, t) = \sum_{n=1}^{\infty} \Xi_n e^{i\omega t} \cos(\alpha x), & \phi_o^t(x, t) = \sum_{n=1}^{\infty} \Theta_n^t e^{i\omega t} \sin(\alpha x), \\ \phi_o^b(x, t) = \sum_{n=1}^{\infty} \Theta_n^b e^{i\omega t} \sin(\alpha x), & \alpha = \frac{n\pi}{L}, \quad i = \sqrt{-1}, \end{cases} \quad (22)$$

where U_n , W_n , Ξ_n , Θ_n^t and Θ_n^b are the unknown maximum coefficients; ω is the natural frequency.

Substituting Eq. (22) into Eq. (21) results in the analytical solution in matrix form as

$$\left(\begin{bmatrix} \mathbf{K}_{qq} & \mathbf{K}_{q\phi} \\ \mathbf{K}_{\phi q} & \mathbf{K}_{\phi\phi} \end{bmatrix} - \omega^2 \begin{bmatrix} \mathbf{M}_{qq} & \mathbf{0} \\ \mathbf{0} & \mathbf{0} \end{bmatrix} \right) \begin{Bmatrix} \mathbf{q}_q \\ \mathbf{q}_\phi \end{Bmatrix} = \begin{Bmatrix} \mathbf{0} \\ \mathbf{0} \end{Bmatrix}, \quad (23)$$

in which

$$\mathbf{K}_{qq} = \begin{bmatrix} k_{qq}^{(11)} & k_{qq}^{(12)} & k_{qq}^{(13)} \\ & k_{qq}^{(22)} & k_{qq}^{(23)} \\ \text{sym.} & & k_{qq}^{(33)} \end{bmatrix}, \quad \mathbf{K}_{q\phi} = -\mathbf{K}_{\phi q}^T = \begin{bmatrix} k_{q\phi}^{(11)} & k_{q\phi}^{(12)} \\ k_{q\phi}^{(21)} & k_{q\phi}^{(22)} \\ k_{q\phi}^{(31)} & k_{q\phi}^{(32)} \end{bmatrix}, \quad \mathbf{K}_{\phi\phi} = \begin{bmatrix} k_{\phi\phi}^{(11)} & k_{\phi\phi}^{(12)} \\ k_{\phi\phi}^{(21)} & k_{\phi\phi}^{(22)} \end{bmatrix}, \quad (24)$$

$$\mathbf{M}_{qq} = \begin{bmatrix} m_{qq}^{(11)} & m_{qq}^{(12)} & m_{qq}^{(13)} \\ & m_{qq}^{(22)} & m_{qq}^{(23)} \\ \text{sym.} & & m_{qq}^{(33)} \end{bmatrix}, \quad \mathbf{q}_q = \begin{Bmatrix} U_n \\ W_n \\ \Xi_n \end{Bmatrix}, \quad \mathbf{q}_\phi = \begin{Bmatrix} \Theta_n^t \\ \Theta_n^b \end{Bmatrix}, \quad (25)$$

$$\begin{cases} k_{qq}^{(11)} = -\alpha^2 A_1, k_{qq}^{(12)} = \alpha^3 B_1, k_{qq}^{(13)} = -\alpha^2 B_s, k_{qq}^{(22)} = -\alpha^4 D, k_{qq}^{(23)} = \alpha^3 D_s, k_{qq}^{(33)} = -\alpha^2 H_s - A_s, \\ k_{q\phi}^{(11)} = \alpha D_1^t, k_{q\phi}^{(12)} = \alpha D_1^b, k_{q\phi}^{(21)} = -\alpha^2 D_2^t, k_{q\phi}^{(22)} = -\alpha^2 D_2^b, k_{q\phi}^{(31)} = \alpha D_3^t, k_{q\phi}^{(32)} = \alpha D_3^b, \\ k_{\phi\phi}^{(11)} = -D_5^t, k_{\phi\phi}^{(12)} = 0, k_{\phi\phi}^{(21)} = 0, k_{\phi\phi}^{(22)} = -D_6^b, \\ m_{qq}^{(11)} = -I_o, m_{qq}^{(12)} = \alpha I_1, m_{qq}^{(13)} = -J_1, m_{qq}^{(22)} = -I_o - \alpha^2 I_2, m_{qq}^{(23)} = \alpha J_2, m_{qq}^{(33)} = -J_3. \end{cases} \quad (26)$$

Eliminating the electric potential vector \mathbf{q}_ϕ , Eq. (23) becomes

$$\left(\mathbf{K}_{qq} - \mathbf{K}_{q\phi} \mathbf{K}_{\phi\phi}^{-1} \mathbf{K}_{\phi q} - \omega^2 \mathbf{M}_{qq} \right) \mathbf{q}_q = \mathbf{0}. \quad (27)$$

3. NUMERICAL EXAMPLES

Geometrical parameters of the beam are $L = 5 \times 10^{-1}$ m, $h_c = 4 \times 10^{-3}$ m, $h_f = 1 \times 10^{-4}$ m; the width of the beam (b) is unity. Mechanical properties of the metal matrix which is Aluminum are $E_m = 70$ GPa, $\rho_m = 2702$ kg/m³, $\mu_m = 0.3$ [12]. Physical properties of piezoelectric which is PZT-G1195N are $E_e = 63$ GPa, $\rho_e = 7600$ kg/m³, $\mu_e = 0.3$, $d_{31} = 254 \times 10^{-12}$ m/V, $p_{33} = 15.0 \times 10^{-9}$ F/m [12, 21], $e_{31} = d_{31} E_e$. Geometrical parameters and mechanical properties of GPLs are $w_{GPL} = 1.5$ μ m, $l_{GPL} = 2.5$ μ m, $t_{GPL} = 1.5$ nm, $E_{GPL} = 1.01$ TPa, $\rho_{GPL} = 1062.5$ kg/m³, $\mu_{GPL} = 0.186$ [7].

In the result presentation, non-dimensional natural frequencies are introduced as

$$\hat{\omega}_i = \left(\omega_i L^2 \sqrt{\rho_m / E_m} \right) / h. \quad (28)$$

3.1. Validation

For the validation purpose, the studied beam is modified to become a single-layer GPL-RP beam by omitting the two piezoelectric layers in the analysis. The natural frequency of this beam was investigated by Priyanka et al. [8] employing quasi-3D theory. Properties and geometries of GPLs are taken as in the material introduction of Section 3. Metal matrix of the porous layer is copper (Cu) which has material properties as $E_{Cu} =$

130 GPa, $\rho_{Cu} = 8960 \text{ kg/m}^3$, $\mu_{Cu} = 0.34$ [8]. Obtained results are reported in Table 1. The data show an excellent agreement between the present study and the study of Priyanka et al. [8]. The results of Priyanka et al. [8] are slightly different from those of present study because quasi-3D theory was employed to model the beam in [8], whereas PSBT, which is a higher-order beam theory, is adopted for the current study.

Table 1. The first non-dimensional frequency $\bar{\omega} = \omega L \sqrt{\rho_{Cu} (1 - \mu_{Cu}^2) / E_{Cu}}$ [8] of single-layer GPL-RP beam ($L/h = 20$, $W_{GPL} = 1 \text{ wt.}\%$)

Source	e_o		
	0.2	0.4	0.6
Present	0.1911	0.1904	0.1905
Priyanka et al. [8]	0.1903	0.1894	0.1893

3.2. Comprehensive studies

Tables 2 and 3 present the first five non-dimensional natural frequencies of the piezoelectric GPL-RP beam with different values of porosity coefficient (e_o) and GPL weight fraction (W_{GPL}), respectively. Two types of electrical boundary condition are taken into consideration, which are closed- and open-circuit conditions. In the case of closed-circuit, the surfaces of the piezoelectric layers are grounded; consequently, the electric potential at the free surface of piezoelectric layers is identically zero. Whereas, in the case of open-circuit, the electric potential difference between the two surfaces of each piezoelectric layer exists; thus, the electromechanical coupling effect happens in the system [18].

Table 2. First five non-dimensional natural frequencies of the piezoelectric GPL-RP beam with the open-/close-circuit electrical boundary conditions and different values of e_o ($W_{GPL} = 0.5 \text{ wt.}\%$)

Frequencies	$e_o = 0$			$e_o = 0.4$			$e_o = 0.8$		
	open	closed	Δ (%)	open	closed	Δ (%)	open	closed	Δ (%)
$\hat{\omega}_1$	3.101	3.061	1.32	3.085	3.038	1.53	3.140	3.084	1.82
$\hat{\omega}_2$	12.399	12.238	1.32	12.333	12.148	1.52	12.551	12.327	1.81
$\hat{\omega}_3$	27.879	27.516	1.32	27.726	27.310	1.52	28.205	27.703	1.81
$\hat{\omega}_4$	49.516	48.870	1.32	49.233	48.495	1.52	50.057	49.169	1.81
$\hat{\omega}_5$	77.272	76.266	1.32	76.813	75.664	1.52	78.045	76.663	1.80

$$\Delta (\%) = \left(\hat{\omega}_i^{\text{open}} - \hat{\omega}_i^{\text{closed}} \right) / \hat{\omega}_i^{\text{closed}} \times 100\%$$

The obtained results in Tables 2 and 3 show that the natural frequencies of the piezoelectric GPL-RP beam with the open-circuit condition are slightly higher than those with the closed-circuit one. The reason is that the electromechanical coupling effect in the beam with the open-circuit condition converts the electric potential to mechanical energy. This finding is similar to the results of Kiani [18], Selim et al. [19] for plate models

covered by piezoelectric layers. Moreover, the relative discrepancy of the frequencies (Δ) between open- and closed-circuit conditions increases with increasing e_o , but decreases with increasing W_{GPL} . In addition, the relative discrepancy Δ of different frequencies for the same values of e_o (Table 2) or W_{GPL} (Table 3) is very small.

Table 3. First five non-dimensional natural frequencies of the piezoelectric GPL-RP beam with the open-/closed-circuit electrical boundary conditions and different values of W_{GPL} ($e_o = 0.5$)

Frequencies	$W_{GPL} = 0$ wt. %			$W_{GPL} = 0.6$ wt. %			$W_{GPL} = 1.2$ wt. %		
	open	closed	Δ (%)	open	closed	Δ (%)	open	closed	Δ (%)
$\hat{\omega}_1$	2.767	2.713	1.98	3.148	3.101	1.528	3.487	3.444	1.25
$\hat{\omega}_2$	11.061	10.847	1.97	12.585	12.396	1.527	13.940	13.768	1.25
$\hat{\omega}_3$	24.867	24.386	1.97	28.291	27.866	1.525	31.335	30.949	1.25
$\hat{\omega}_4$	44.158	43.305	1.97	50.232	49.479	1.523	55.631	54.946	1.25
$\hat{\omega}_5$	68.898	67.569	1.97	78.362	77.188	1.520	86.771	85.706	1.24

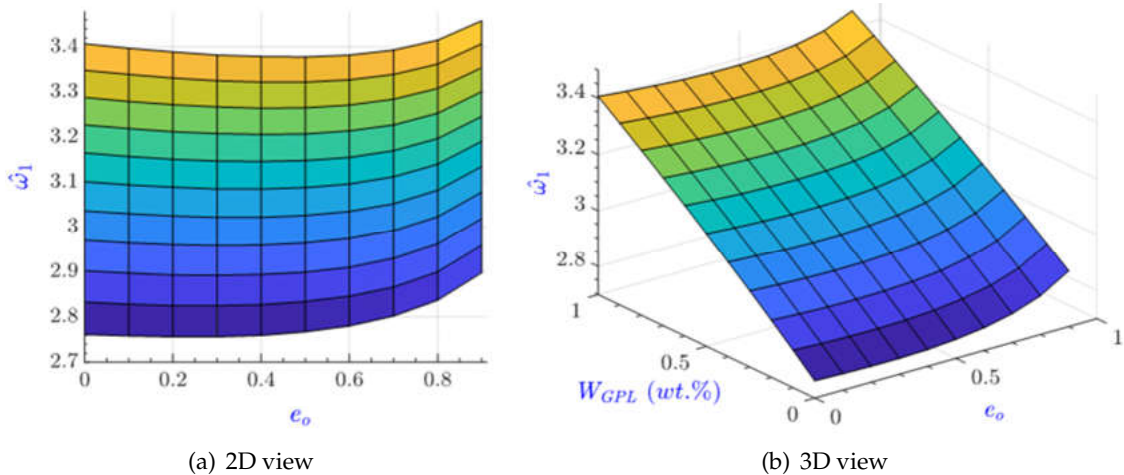
$$\Delta (\%) = \left(\hat{\omega}_i^{\text{open}} - \hat{\omega}_i^{\text{closed}} \right) / \hat{\omega}_i^{\text{closed}} \times 100\%$$


Fig. 2. Effect of porosity coefficient (e_o) and GPL weight fraction (W_{GPL}) on the first non-dimensional natural frequency of the piezoelectric GPL-RP beam (open-circuit condition)

The 3D plot in Fig. 2 illustrates the influence of porosity coefficient (e_o) and GPL weight fraction (W_{GPL}) on the first non-dimensional natural frequency of the piezoelectric GPL-RP beam. Observing Fig. 2 as well as the data in Tables 2 and 3 shows that (1) when W_{GPL} increases, the frequency usually increases; (2) when e_o increases, the variation of the frequency is quite complicated. The frequency slightly decreases and then increases with respect to e_o . This is because the increase of e_o reduces both the effective mass density and the stiffness of the beam. Hence, the complex development of the

frequency is due to the correlation effect between the stiffness and mass matrices of the system when e_o increases. In other words, the increase of e_o does not always induce the decrease of natural frequency, it seems due to the relative relation between mass effect and stiffness effect.

4. CONCLUSIONS AND REMARKS

Navier's solution for the natural frequency analysis of the piezoelectric GPL-RP beam is presented. In the modelling, the symmetrical distributions of both porosity and GPLs in the porous core are supposed. The effective mechanical properties of the GPL-RP core are estimated via Halpin-Tsai model and the rule of mixture. The electric potential is assumed to vary linearly across each piezoelectric layer thickness. PSBT associated with Hamilton's principle is employed to derive the governing equations of motion. The effects of parameters and conditions, including GPL weight fraction, porosity coefficient and electrical boundary conditions on the natural frequencies of the beam are investigated and discussed. The studied results for piezoelectric GPL-RP beam are initial; further work is going on to explore the electromechanical coupling effect on controlling the mechanical behavior of the beam.

DECLARATION OF COMPETING INTEREST

The authors declare that they have no known competing financial interests or personal relationships that could have appeared to influence the work reported in this paper.

ACKNOWLEDGEMENT

This work was supported by The University of Danang, University of Science and Technology, code number of project: B2022-DN02-08.

REFERENCES

- [1] M. R. Barati and A. M. Zenkour. Analysis of postbuckling of graded porous GPL-reinforced beams with geometrical imperfection. *Mechanics of Advanced Materials and Structures*, **26**, (2018), pp. 503–511. <https://doi.org/10.1080/15376494.2017.1400622>.
- [2] M. R. Barati and A. M. Zenkour. Post-buckling analysis of refined shear deformable graphene platelet reinforced beams with porosities and geometrical imperfection. *Composite Structures*, **181**, (2017), pp. 194–202. <https://doi.org/10.1016/j.compstruct.2017.08.082>.
- [3] M. Ganapathi, B. Anirudh, C. Anant, and O. Polit. Dynamic characteristics of functionally graded graphene reinforced porous nanocomposite curved beams based on trigonometric shear deformation theory with thickness stretch effect. *Mechanics of Advanced Materials and Structures*, **28**, (2019), pp. 741–752. <https://doi.org/10.1080/15376494.2019.1601310>.
- [4] K. Gao, D. M. Do, R. Li, S. Kitipornchai, and J. Yang. Probabilistic stability analysis of functionally graded graphene reinforced porous beams. *Aerospace Science and Technology*, **98**, (2020). <https://doi.org/10.1016/j.ast.2020.105738>.
- [5] S. Sahmani, M. M. Aghdam, and T. Rabczuk. Nonlinear bending of functionally graded porous micro/nano-beams reinforced with graphene platelets based upon nonlocal strain gradient theory. *Composite Structures*, **186**, (2018), pp. 68–78. <https://doi.org/10.1016/j.compstruct.2017.11.082>.

- [6] B. Anirudh, M. Ganapathi, C. Anant, and O. Polit. A comprehensive analysis of porous graphene-reinforced curved beams by finite element approach using higher-order structural theory: Bending, vibration and buckling. *Composite Structures*, **222**, (2019). <https://doi.org/10.1016/j.compstruct.2019.110899>.
- [7] S. Kitipornchai, D. Chen, and J. Yang. Free vibration and elastic buckling of functionally graded porous beams reinforced by graphene platelets. *Materials & Design*, **116**, (2017), pp. 656–665. <https://doi.org/10.1016/j.matdes.2016.12.061>.
- [8] R. Priyanka, C. M. Twinkle, and J. Pitchaimani. Stability and dynamic behavior of porous FGM beam: influence of graded porosity, graphene platelets, and axially varying loads. *Engineering with Computers*, **38**, (2021), pp. 4347–4366. <https://doi.org/10.1007/s00366-021-01478-5>.
- [9] H. Xu, Y. Q. Wang, and Y. Zhang. Free vibration of functionally graded graphene platelet-reinforced porous beams with spinning movement via differential transformation method. *Archive of Applied Mechanics*, **91**, (2021), pp. 4817–4834. <https://doi.org/10.1007/s00419-021-02036-7>.
- [10] F. Kiarasi, M. Babaei, P. Sarvi, K. Asemi, M. Hosseini, and M. Omidi Bidgoli. A review on functionally graded porous structures reinforced by graphene platelets. *Journal of Computational Applied Mechanics*, **52**, (4), (2021), pp. 731–750.
- [11] S. Zhao, Z. Zhao, Z. Yang, L. Ke, S. Kitipornchai, and J. Yang. Functionally graded graphene reinforced composite structures: A review. *Engineering Structures*, **210**, (2020). <https://doi.org/10.1016/j.engstruct.2020.110339>.
- [12] N. V. Nguyen, J. Lee, and H. Nguyen-Xuan. Active vibration control of GPLs-reinforced FG metal foam plates with piezoelectric sensor and actuator layers. *Composites Part B: Engineering*, **172**, (2019), pp. 769–784. <https://doi.org/10.1016/j.compositesb.2019.05.060>.
- [13] L. B. Nguyen, N. V. Nguyen, C. H. Thai, A. M. J. Ferreira, and H. Nguyen-Xuan. An isogeometric Bézier finite element analysis for piezoelectric FG porous plates reinforced by graphene platelets. *Composite Structures*, **214**, (2019), pp. 227–245. <https://doi.org/10.1016/j.compstruct.2019.01.077>.
- [14] N. V. Nguyen, L. B. Nguyen, H. Nguyen-Xuan, and J. Lee. Analysis and active control of geometrically nonlinear responses of smart FG porous plates with graphene nanoplatelets reinforcement based on Bézier extraction of NURBS. *International Journal of Mechanical Sciences*, **180**, (2020). <https://doi.org/10.1016/j.ijmecsci.2020.105692>.
- [15] Y. X. Hao, H. Li, W. Zhang, X. S. Ge, S. W. Yang, and Y. T. Cao. Active vibration control of smart porous conical shell with elastic boundary under impact loadings using GDQM and IQM. *Thin-Walled Structures*, **175**, (2022). <https://doi.org/10.1016/j.tws.2022.109232>.
- [16] S. C. Tjong. Recent progress in the development and properties of novel metal matrix nanocomposites reinforced with carbon nanotubes and graphene nanosheets. *Materials Science and Engineering: R: Reports*, **74**, (2013), pp. 281–350. <https://doi.org/10.1016/j.mser.2013.08.001>.
- [17] T. R. C. Chuaqui and C. M. C. Roque. Analysis of functionally graded piezoelectric Timoshenko smart beams using a multiquadric radial basis function method. *Composite Structures*, **176**, (2017), pp. 640–653. <https://doi.org/10.1016/j.compstruct.2017.05.062>.
- [18] Y. Kiani. Free vibration of functionally graded carbon nanotube reinforced composite plates integrated with piezoelectric layers. *Computers & Mathematics with Applications*, **72**, (2016), pp. 2433–2449. <https://doi.org/10.1016/j.camwa.2016.09.007>.

- [19] B. A. Selim, L. W. Zhang, and K. M. Liew. Active vibration control of FGM plates with piezoelectric layers based on Reddy's higher-order shear deformation theory. *Composite Structures*, **155**, (2016), pp. 118–134. <https://doi.org/10.1016/j.compstruct.2016.07.059>.
- [20] J. Tian, Q. Guo, and G. Shi. Laminated piezoelectric beam element for dynamic analysis of piezolaminated smart beams and GA-based LQR active vibration control. *Composite Structures*, **252**, (2020). <https://doi.org/10.1016/j.compstruct.2020.112480>.
- [21] P. Phung-Van, T. Nguyen-Thoi, T. Le-Dinh, and H. Nguyen-Xuan. Static and free vibration analyses and dynamic control of composite plates integrated with piezoelectric sensors and actuators by the cell-based smoothed discrete shear gap method (CS-FEM-DSG3). *Smart Materials and Structures*, **22**, (2013). <https://doi.org/10.1088/0964-1726/22/9/095026>.